LETTER

PHYSICAL REVIEW APPLIED 7, 041002 (2017)

Effects of Charge Balance and Exciton Confinement on the Operational Lifetime of Blue Phosphorescent Organic Light-Emitting Diodes

Caleb Coburn[1] and Stephen R. Forrest[1,2]

[1]*Department of Physics, University of Michigan, Ann Arbor, Michigan 48109, USA*

[2]*Departments of Electrical Engineering and Computer Science, and Materials Science and Engineering, University of Michigan, Ann Arbor, Michigan 48109, USA*

(Received 19 January 2017; revised manuscript received 1 March 2017; published 24 April 2017)

We measure the contribution of loss of charge balance and exciton confinement in the emission zone to the operational lifetime of blue phosphorescent organic light-emitting diodes (PHOLEDs). Charge balance and exciton confinement are monitored as functions of time by measuring the emission intensity of either phosphorescent or fluorescent red-emitting "sensing" layers embedded within the charge-transport layers outside of the emission zone. We find no significant change in charge balance over the lifetime of the device, while loss of exciton confinement accounts for $<5\%$ of luminance loss, confirming that degradation is primarily due to decomposition of molecular constituents within the emission layer of the PHOLED.

DOI: 10.1103/PhysRevApplied.7.041002

The reliability of phosphorescent organic light-emitting diodes (PHOLEDs) is crucial to their usefulness in displays [1] and lighting [2]. Unlike that of red or green devices, the operational lifetime of blue PHOLEDs is too short for most practical applications. Studies of blue PHOLED lifetimes have focused primarily on degradation of the emission layer (EML) [3–6]; however, the loss of luminance due to degradation in other layers may also contribute. For example, blue PHOLED lifetime is affected by changes in the charge balance efficiency η_{CB} defined as the ratio of excitons formed in the EML to the number of charges injected. The device lifetime is also affected by the loss of exciton confinement η_{EC} defined as the percentage of excitons generated in the EML that recombine without diffusing into adjacent layers. Thus, degradation of blocking layers, changes in layer morphology, or increased resistance can decrease the device luminous efficiency by reducing either η_{CB} or η_{EC}.

Here, we employ red δ-doped (i.e., ultrathin) "sensing layers" in the charge-transport regions to monitor changes in η_{CB} and η_{EC} of a blue PHOLED over its operational lifetime [5,7,8]. Charge and triplet exciton leakage are distinguished by comparing the emission intensities from the fluorescent vs phosphorescent sensing layers. Using this technique, we find that changes in exciton confinement account for $<5\%$ of luminance loss, while changes in charge balance do not contribute significantly. This confirms that degradation of molecular species primarily occurs within the emission layer itself.

To measure charge and exciton leakages from the EML, we fabricate devices having red-emitting phosphorescent or fluorescent sensor molecules doped into the electron-transport layer (ETL) or hole-transport layer (HTL). Assuming that phosphorescent sensing layers efficiently collect all leaked charges and excitons, the charge balance efficiency is determined from the ratio sensor emission to injected charges via

$$\eta_{\mathrm{CB}}\eta_{\mathrm{EC}} = 1 - q\Phi_p/J\eta_{\mathrm{OC}}\chi\Phi_{\mathrm{PLQY}}, \tag{1}$$

where q is the electron charge, J is the current density, Φ_p is the outcoupled photon flux emitted by the sensing layer, η_{OC} is the sensor layer optical outcoupling efficiency, χ is the fraction of emissive excitons (i.e., $\chi = 1$ for a phosphorescent sensor and ¼ for a fluorescent sensor), and Φ_{PLQY} is the photoluminescent quantum yield of the sensor. Excitons formed in the EML rapidly intersystem cross on phosphorescent dopant molecules to form emissive triplets. Because triplet excitons on the fluorescent sensor are nonemissive at room temperature, these sensing layers only emit via singlet excitons directly formed by leaked charges or by Förster transfer from the EML. In the absence of Förster transfer, fluorescent sensing layers are sensitive only to charge leakage, and $\eta_{\mathrm{EC}} = 1$ in Eq. (1). Thus, phosphorescent sensing layers measure both charge and exciton leakage, while fluorescent sensing layers decouple these two by measuring charge leakage separately.

To avoid changing the device characteristics due to trapping of holes in the HTL or electrons in the ETL, sensor materials should have a deeper highest occupied molecular orbital (HOMO) energy (measured from the vacuum level) than the HTL and a shallower lowest unoccupied molecular orbital (LUMO) energy than the ETL. Additionally, the sensing material luminescence should be easily spectrally resolved from that of the dopant.

Three sensing devices—Pt (II) octaethylporphine (PtOEP) HTL and ETL sensing, and 4-(dicyanomethylene)-6-methyl-2-[2-(julolidin-9-yl)ethenyl]-4*H*-pyran (DCM2) ETL sensing—are grown by vacuum thermal evaporation (VTE) at a base pressure $<5\times10^{-7}$ torr on solvent-cleaned substrates comprising a prepatterned, 70-nm-thick indium tin oxide (ITO, $60\pm10\ \Omega/\mathrm{sq}$) layer on glass. The substrates are exposed to UV ozone for 10 min

 © 2017 American Physical Society

immediately prior to loading into the VTE chamber. The 2-mm^2 device area is defined by the intersection of the ITO anode and the 100-nm-thick Al cathode, the latter layer patterned by deposition through a shadow mask. The device structure for the PtOEP ETL sensing device is ITO anode/10-nm hexaazatriphenylene hexacarbonitrile hole injection layer/20-nm N,N'-bis(naphthalen-1-yl)-N,N'-bis(phenyl)-2, 2′-dimethylbenzidine (NPD) HTL/30-nm 4,40-bis(3-methylcarbazol-9-yl)-2, 20-biphenyl- (mCBP) doped 13 vol % with Ir (III) tris[3-(2,6-dimethylphenyl)-7-methylimidazo[1,2-f]-phenanthridine] [$Ir(dmp)_3$] EML/6-nm mCBP hole and exciton blocking layer (HBL)/30-nm Alq_3 ETL/1.5-nm 8-hydroxyquinolinato Li electron injection layer/cathode. The 2-nm-thick Alq_3 layer immediately adjacent to the mCBP HBL is doped at 8 vol % with the red phosphor, PtOEP. The DCM2 ETL sensing device differs only by using a 0.05-nm-thick layer of DCM2 located 10 nm from the EML. The structure for the PtOEP HTL sensing device is the same as above except that the HTL consists of a 20-nm-thick di(phenyl-carbazole)-N,N'-bis-phenyl-(1,1′-biphenyl)-4,4′-diamine (CPD) doped with a 0.1-nm-thick PtOEP layer located 6 nm from the EML, with no sensor on the ETL side. The device structures are shown schematically in Fig. 1(a), along with the approximate transport levels of the materials. Each device has a single sensing layer, and in the ETL sensing devices, CPD is replaced with NPD. The sensing layers are located sufficiently far from the EML to avoid direct Förster energy transfer from the blue dopant, $Ir(dmp)_3$. The transfer radii from $Ir(dmp)_3$ to PtOEP and DCM2 are 3.5 and 3.9 nm, respectively, calculated using the sensor absorption spectra in Refs. [9–11]. The layer thicknesses controlled using a crystal microbalance are accurate to within 5%.

PtOEP is chosen as the phosphorescent sensing material since its low triplet energy ($E_T = 1.9$ eV) allows efficient energy transfer from Alq_3 [12,13] ($E_T = 2.1 \pm 0.1$ eV). Also, its LUMO energy is aligned with that of Alq_3 [14], while the HOMO level (5.3 ± 0.1) is approximately 0.5 eV higher than Alq_3 (5.8 ± 0.2 eV). Hence, PtOEP traps holes but not electrons in the ETL [12,14]. On the other hand, CPD has a HOMO energy of 5.5 ± 0.1 eV, and its LUMO energy is expected to be similar to NPD (approximately 1.5 eV). Therefore, only electrons are trapped on PtOEP in CPD, with the PtOEP LUMO at 0.5 eV below that of the CPD, while the HOMO energies are aligned to within 0.2 eV, as shown in Fig. 1(a). The DCM2 HOMO is 5.3 eV, whereas its LUMO is 0.4 ± 0.1 eV below that of Alq_3 and can trap electrons [15], although we find δ-doped layers cause no change in the device operating characteristics.

Following fabrication, the PHOLEDs are encapsulated in ultrapure nitrogen (<0.5 ppm oxygen and water concentration) using a glass slide sealed to the substrate with UV-cured epoxy applied around its periphery. The current-voltage luminance characteristics of the packaged devices are measured immediately following fabrication. Two of each device type are life tested at a current density of 30 mA/cm^2, and the electroluminescence spectra are measured at $J = 1$ and 10 mA/cm^2 each time the devices degrade by approximately 5% of their initial luminance (at times corresponding to T100, T95, T90, etc.).

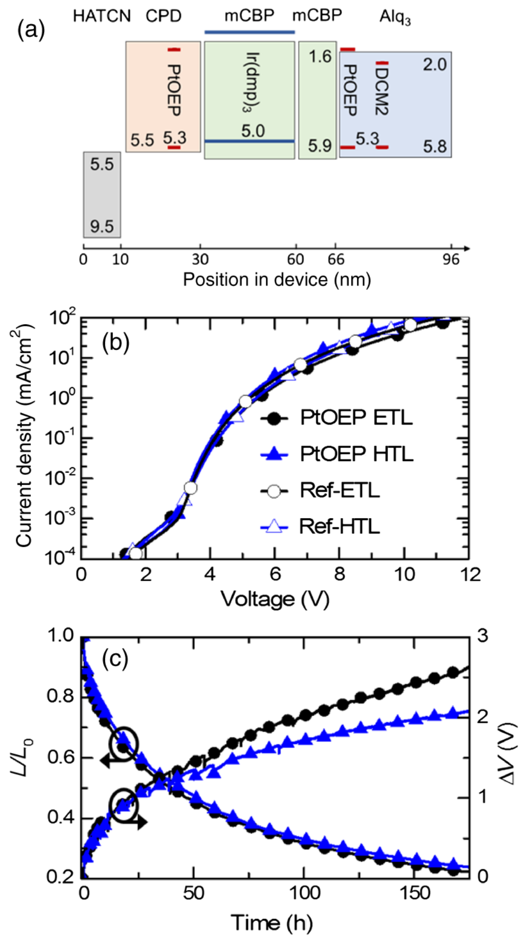

FIG. 1. (a) Energy-level diagram of the PHOLEDs. Energies listed are in eV from the vacuum level. Note that for the ETL-side sensing devices, the HTL is NPD rather than CPD. Each device contains a single sensing layer. (b) Current-density vs voltage characteristics of the as-grown devices. The reference devices omit sensing layers but are otherwise unchanged. (c) Luminance (L) normalized to its initial value (L_0) and voltage rise (ΔV) vs operating time at 30 mA/cm^2 for PtOEP HTL- and ETL-side sensing devices.

Films with structures of 25-nm-thick Alq_3 doped with 8 vol % PtOEP, 5 nm CPD/0.1 nm PtOEP/5 nm CPD/0.1 nm PtOEP/5 nm CPD, and 5 nm Alq_3/0.05 nm DCM2/5 nm Alq_3/0.05 nm DCM2/5 nm Alq_3 are deposited on quartz substrates for PLQY measurements of the sensing layers. The measurements are carried out in an integrating sphere under nitrogen flow and illuminated with a HeCd laser at a wavelength of 325 nm.

The PLQY of the PtEOP:Alq_3 film is $14.9 \pm 1.6\%$, PtOEP:CPD film $28.5 \pm 1.9\%$, and DCM2:Alq_3 film $50 \pm 9\%$. The percentage of emissive excitons at the sensing layers that emit outcoupled photons is determined using Green's function methods [16] along with the indexes

of the refraction of the layers measured by ellipsometry. The percentage of outcoupled photons for the PtOEP ETL sensing layer is $\eta_{OC}\Phi_{QY}100\% = 2.3 \pm 0.2\%$, PtOEP HTL $5.1 \pm 0.2\%$, and DCM2-ETL $7.5 \pm 1.4\%$.

The current-density–voltage (J-V) characteristics of the PtOEP ETL and PtOEP HTL sensing devices along with those for the reference devices without sensing layers are given in Fig. 1(b). The performance is similar for all device types, with small differences due to the different HTL materials used and unavoidable growth-to-growth variations. The DCM2 ETL sensing device J-V characteristic is also comparable to its reference. The peak external quantum efficiency of the devices is 8.8%. The luminance loss and voltage rise over time at $J = 30\ \mathrm{mA/cm^2}$ are given in Fig. 1(c) for the PtOEP HTL and ETL sensing devices. All devices show the same lifetime and voltage rise behaviors, independent of the sensing layers employed.

As the device ages, the emission intensity of the PtOEP ETL sensing layer increases [Fig. 2(a)], whereas it decreases for the PtOEP HTL sensing layer [Fig. 2(b)]. The sensor intensity is obtained by subtracting the aged reference and sensing device spectra (Fig. 2, detail). Unlike the PtOEP ETL sensing layer, the DCM2 emission does not change with device age, (see Fig. 2). Care must be taken to avoid saturation of the thin δ-doped sensor layers which could occur at high current densities due to the long (approximately 100 μs) lifetime of PtOEP phosphorescence [17]. The site saturation limit is determined using $k_r N \approx \Phi_p/(\eta_{OC}\eta_\chi\Phi_{PLQY})$, where k_r is the radiative recombination rate and N is the number of sensor molecules. At $J = 10\ \mathrm{mA/cm^2}$, the sensing layer emission is approximately 100 times lower than the point when every PtOEP molecule is excited.

The fraction of charge injected to charge leakage from the EML is $1 - \eta_{CB}\eta_{EC}$ calculated using the phosphorescent sensing spectra, with results shown in Fig. 3. The leakage into the ETL is shown in Fig. 3(a). It increases as the device ages and is an approximately linear function of the fraction of loss in luminance (L) from its initial value (L_0), i.e., L/L_0. The differences in leakage at $J = 1$ and $10\ \mathrm{mA/cm^2}$ are due to shifts in the charge recombination zone from the ETL to the HTL side of the EML [7]. Leakage leads to proportionately larger sensor emission at low currents at the ETL side, whereas the HTL-side leakage does not change over the same range of current [see Fig. 3(b)].

Comparing the behavior of the sensor emission vs aging time for the ETL sensing layers in Figs. 2(a) and 2(c), we see that the PtOEP emission increases while the DCM2 emission is constant. Because the DCM2 sensing data are only sensitive to charge leakage, we conclude that charge balance does not change as the device degrades. The increased emission from the PtOEP ETL sensing layer is, therefore, attributed to increased leakage of triplet excitons into the ETL.

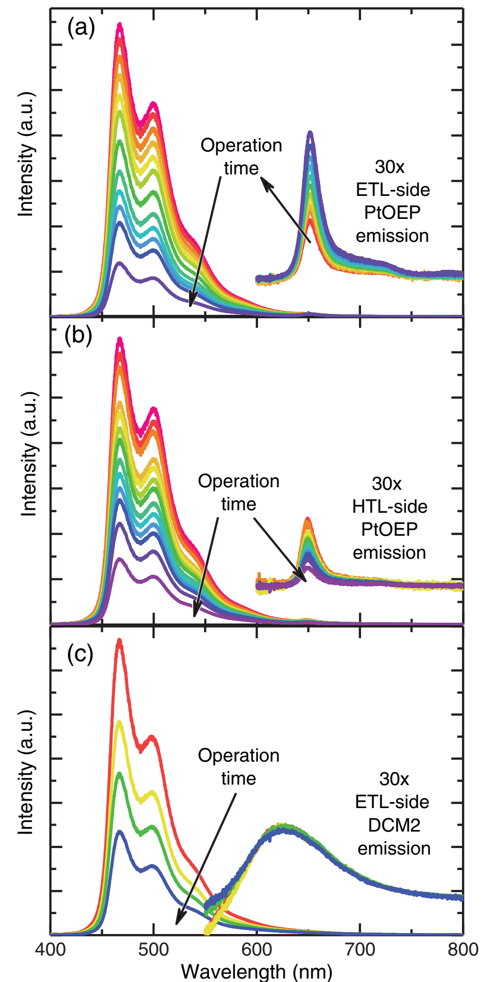

FIG. 2. (a) PtOEP ETL sensing device spectra. The intensity of the blue phosphorescent emission at wavelengths from 450 to 550 nm decreases with time while the sensor emission at 650 nm increases, indicating increasing exciton diffusion into the ETL. Data correspond to operating times of 0, 0.1, 1.2, 3.3, 6.7, 11.4, 22.6, 39.5, 55.1, 71.7, 95.3, and 214 h. (b) PtOEP HTL sensing device spectra. The sensing layer emission intensity decreases with time, indicating reduced leakage on the HTL side. Data correspond to operating times of 0, 0.4, 1.5, 3.5, 8.0, 11.0, 16.4, 20.7, 30.1, 39.1, 59.2, 88.9, and 179 h. (c) DCM2 ETL sensing device spectra. The emission intensity is constant with time, indicating no change in hole penetration into the ETL. Data correspond to operating times of 0, 0.3, 42.8, and 109 h. Sensor emission magnified by 30x and vertically offset for clarity is shown in the detail of (a)–(c).

Exciton blocking at the EML-HBL interface relies on the high $E_T = 2.95$ eV of mCBP [18] relative to $\mathrm{Ir(dmp)_3}$ ($E_T = 2.7 \pm 0.1$ eV). A possible cause of the increased exciton leakage includes chemical degradation that results in low triplet energy degradation products in the HBL. Several degradation products of mCBP have been identified with smaller energy gaps and likely lower triplet energies than mCBP [19]. Morphological changes of the blocking layers have also been linked to degradation of organic photovoltaic devices [20]. For example, crystallite

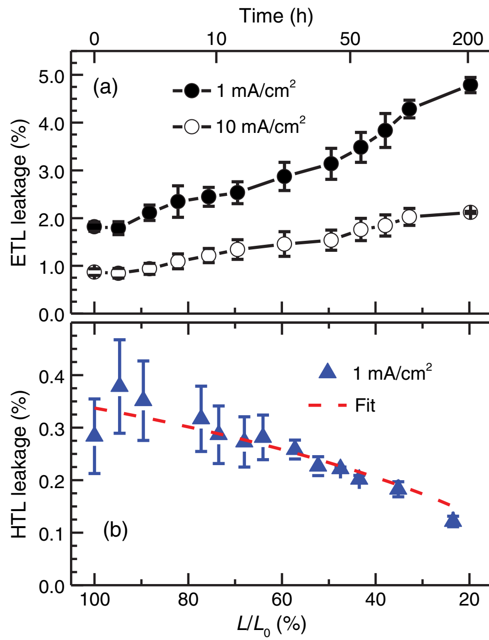

FIG. 3. Percent leakage $100\%(1-\eta_{CB}\eta_{EC})$ on (a) the ETL at $J = 1$ and 10 mA/cm^2 and (b) HTL sides of the blue PHOLED vs the percent luminance loss, L/L_0. The dashed line is a fit to the HTL-side leakage. The HTL leakage decreases with time and is the same at $J = 1$ and 10 mA/cm^2 (not shown). The error bars represent the differences between two samples of each device type.

formation in the HBL can intermix the HBL and ETL layers, reducing their exciton blocking efficiencies.

Electron leakage into the HTL of analogous devices is attributed to exciton diffusion [7,21] that results from the low triplet energy of the HTL compared to the EML constituents. In addition, both NPD and CPD fluoresce in the wavelength range $\lambda = 400$–500 nm [21]. This fluorescence is not observed here; thus we conclude that emission from the HTL sensing layer is also due to exciton diffusion.

Quenching at defects reduces the lifetime and diffusion length of excitons within degraded EMLs. Additionally, increased nonradiative recombination of charges on defects reduces the exciton formation rate. These effects cause a decrease in the exciton flux into the HTL. We quantitatively determine the decrease in exciton flux by solving the diffusion equation together with the PHOLED degradation model based on the hot triplet annihilation of Ref [4]. Specifically, we solve

$$\frac{d}{dt}T(x,t,t') = \frac{d}{dx}\left[D(x)\frac{d}{dx}T(x,t,t')\right] + G(x,t') - \frac{1}{\tau(t')}T(x,t,t'), \qquad (2)$$

where x is the position in the device, t is the time for triplet diffusion and transport (on the order of microseconds), t' is the operation time leading to generation of defects (tens to thousands of hours), $T(x,t,t')$ is the triplet density, $D(x)$ is the diffusivity, $G(x,t')$ is the exciton generation rate normalized to that of the fresh device, and $\tau(t')$ is the exciton lifetime. The exciton density is zero at the sensing layer, corresponding to exciton trapping on sensor molecules, and excitons are blocked at the HBL. We use $D = 2.3\times10^{-7}$ cm^2 s^{-1} and $\tau = 100$ μs for exciton diffusion and lifetime in the HTL and 7.6×10^{-7} cm^2 s^{-1} for the EML [7]. The values for $\tau(t')$ range from 1.1 μs at $L/L_0 = 1.0$ to 0.5 μs at $L/L_0 = 0.16$ [4], with values intermediate to the measurements obtained by linear interpolation. Finally, the dependence of G on t' is found by solving Eqs. (1)–(3) and (4d) of Ref. [4], simplified by assuming a uniform exciton generation zone and using the corresponding parameter values in Table 1 of Ref. [4] for the hole and electron densities $p(t,t')$ and $n(t,t')$, respectively. The normalized exciton generation rate inside the EML is then $p(\infty,t')n(\infty,t')/[p(\infty,0)p(\infty,0)]$ and zero elsewhere. The exciton flux at the sensing layer is $D(x)dT(x,\infty,t')/dx$ evaluated at the position of the sensing layer.

The resulting change in exciton flux at the HTL sensor layer relative to the as-grown device is shown in Fig. 3 (dashed line) scaled to match the PtOEP HTL sensing data. The agreement between the HTL emission data and theory support the conclusion that reduced exciton leakage into the HTL results from reduced diffusion due to EML degradation.

The contribution of loss of charge balance and exciton confinement to the luminance decrease is

$$\Delta L_{CB}(t') = 100\%\{1-[\eta_{CB}(t')\eta_{EC}(t') - \eta_{CB}(0)\eta_{EC}(0)]\}/(1-L/L_0) \qquad (3)$$

calculated using the PtOEP sensing data with results shown in Fig. 4. Here, the error bars represent the difference in $\Delta L_{CB}(t')$ calculated for similar devices. The loss of exciton confinement accounts for approximately 3% of luminance loss at $J = 1$ mA/cm^2 and 1%–2% at 10 mA/cm^2. This implies that 97% of luminance loss is due to the degradation of molecular species in the EML itself, consistent

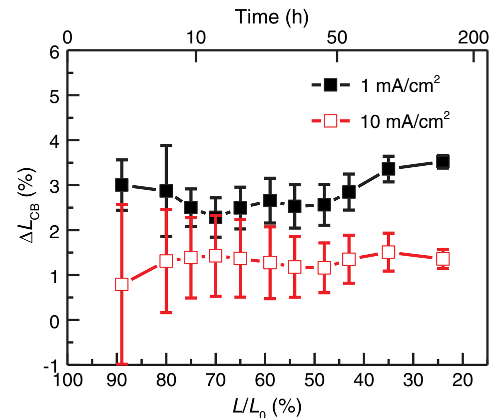

FIG. 4. Percentage contribution of loss of charge balance and exciton confinement to luminance loss $\Delta L_{CB}(t')$ vs the percentage of luminance loss L/L_0 and operating time (top axis).

with assumptions in previous investigations of the lifetime of blue-emitting PHOLEDs [4,5,22].

In summary, we find that loss of exciton confinement contributes approximately 3% to the luminance loss in blue PHOLEDs over their operational lifetimes, while charge balance is not significantly changed. We reach this conclusion by direct measurement of the luminance from red-emitting sensing layers located within the electron- and hole-transport layers. Indeed, over 95% of the luminance loss in these devices occurs by direct aging of the dopants and/or hosts in the EML. Based on these findings, further improvements in lifetime will require more robust hosts, emitters, or other strategies for reducing their degradation pathways [5,8,23,24].

The authors thank J. Lee and T. Fleetham for measuring the energetics of CPD, mCBP and NPD and Y. Qu for assistance with the outcoupling calculations. This work is supported by the Department of Energy Solid State Lighting Program (Contract No. DE-EE000707), the Air Force Office of Scientific Research, and Universal Display Corporation.

[1] B. Geffroy, P. Le Roy, and C. Prat, Organic light-emitting diode (OLED) technology: Materials, devices and display technologies, Polym. Int. **55**, 572 (2006).
[2] H. Sasabe and J. Kido, Development of high performance OLEDs for general lighting, J. Mater. Chem. C **1**, 1699 (2013).
[3] Q. Wang and H. Aziz, Degradation of organic/organic interfaces in organic light-emitting devices due to polaron-exciton interactions, ACS Appl. Mater. Interfaces **5**, 8733 (2013).
[4] N. C. Giebink, B. W. D'Andrade, M. S. Weaver, P. B. Mackenzie, J. J. Brown, M. E. Thompson, and S. R. Forrest, Intrinsic luminance loss in phosphorescent small-molecule organic light emitting devices due to bimolecular annihilation reactions, J. Appl. Phys. **103**, 044509 (2008).
[5] Y. F. Zhang, J. Lee, and S. R. Forrest, Tenfold increase in the lifetime of blue phosphorescent organic light-emitting diodes, Nat. Commun. **5**, 5008 (2014).
[6] H. Aziz, Z. D. Popovic, N. X. Hu, A. M. Hor, and G. Xu, Degradation mechanism of small molecule-based organic light-emitting devices, Science **283**, 1900 (1999).
[7] C. Coburn, J. Lee, and S. R. Forrest, Charge balance and exciton confinement in phosphorescent organic light emitting diodes, Adv. Opt. Mater. **4**, 889 (2016).
[8] N. C. Erickson and R. J. Holmes, Investigating the role of emissive layer architecture on the exciton recombination zone in organic light-emitting devices, Adv. Funct. Mater. **23**, 5190 (2013).
[9] A. K. Bansal, W. Holzer, A. Penzkofer, and T. Tsuboi, Absorption and emission spectroscopic characterization of platinum-octaethyl-porphyrin (PtOEP), Chem. Phys. **330**, 118 (2006).
[10] V. G. Kozlov, P. E. Burrows, G. Parthasarathy, and S. R. Forrest, Optical properties of molecular organic semiconductor thin films under intense electrical excitation, Appl. Phys. Lett. **74**, 1057 (1999).
[11] V. G. Kozlov, G. Parthasarathy, P. E. Burrows, V. B. Khalfin, J. Wang, S. Y. Chou, and S. R. Forrest, Structures for organic diode lasers and optical properties of organic semiconductors under intense optical and electrical excitations, IEEE J. Quantum Electron. **36**, 18 (2000).
[12] M. A. Baldo, D. F. O'Brien, Y. You, A. Shoustikov, S. Sibley, M. E. Thompson, and S. R. Forrest, Highly efficient phosphorescent emission from organic electroluminescent devices, Nature (London) **395**, 151 (1998).
[13] H. D. Burrows, M. Fernandes, J. S. de Melo, A. P. Monkman, and S. Navaratnam, Characterization of the triplet state of tris(8-hydroxyquinoline)aluminium(III) in benzene solution, J. Am. Chem. Soc. **125**, 15310 (2003).
[14] A. J. Makinen, I. G. Hill, and Z. H. Kafafi, Vacuum level alignment in organic guest-host systems, J. Appl. Phys. **92**, 1598 (2002).
[15] F. Nuesch, D. Berner, E. Tutis, M. Schaer, C. Ma, X. Wang, B. Zhang, and L. Zuppiroli, Doping-induced charge trapping in organic light-emitting devices, Adv. Funct. Mater. **15**, 323 (2005).
[16] K. Celebi, T. D. Heidel, and M. A. Baldo, Simplified calculation of dipole energy transport in a multilayer stack using dyadic Green's functions, Opt. Express **15**, 1762 (2007).
[17] M. A. Baldo and S. R. Forrest, Transient analysis of organic electrophosphorescence: I. Transient analysis of triplet energy transfer, Phys. Rev. B **62**, 10958 (2000).
[18] H. Nakanotani, K. Masui, J. Nishide, T. Shibata, and C. Adachi, Promising operational stability of high-efficiency organic light-emitting diodes based on thermally activated delayed fluorescence, Sci. Rep. **3**, 2127 (2013).
[19] A. S. D. Sandanayaka, T. Matsushima, and C. Adachi, Degradation mechanisms of organic light-emitting diodes based on thermally activated delayed fluorescence molecules, J. Phys. Chem. C **119**, 23845 (2015).
[20] B. Song, Q. C. Burlingame, K. Lee, and S. R. Forrest, Reliability of mixed-heterojunction organic photovoltaics grown via organic vapor phase deposition, Adv. Energy Mater. **5**, 1401952 (2015).
[21] K. Goushi, R. Kwong, J. J. Brown, H. Sasabe, and C. Adachi, Triplet exciton confinement and unconfinement by adjacent hole-transport layers, J. Appl. Phys. **95**, 7798 (2004).
[22] N. C. Giebink, B. W. D'Andrade, M. S. Weaver, J. J. Brown, and S. R. Forrest, Direct evidence for degradation of polaron excited states in organic light emitting diodes, J. Appl. Phys. **105**, 124514 (2009).
[23] D. P. K. Tsang and C. Adachi, Operational stability enhancement in organic light-emitting diodes with ultrathin Liq interlayers, Sci. Rep. **6**, 22463 (2016).
[24] T. B. Fleetham, L. Huang, K. Klimes, J. Brooks, and J. Li, Tetradentate Pt(II) complexes with 6-membered chelate rings: A new route for stable and efficient blue organic light emitting diodes, Chem. Mater. **28**, 3276 (2016).